Research Article

Journal of Applied Material Science & Engineering Research

Solid-state Synthesis of Composite Structures of Various Cu(I)-based Oxides with g-C_3N_4 for Harvesting Solar Energy

Dilshad Masih, Bushra Luzon, Yuanyu Ma, and Sohrab Rohani*

Department of Chemical and Biochemical Engineering, University of Western Ontario, London, ON, Canada

***Corresponding author**
Sohrab Rohani, Department of Chemical and Biochemical Engineering, University of Western Ontario, London, ON, Canada, Tel: +1 (519) 661-4116; E-mail: srohani@uwo.ca

Submitted: 14 Nov 2018; **Accepted**: 21 Nov 2018; **Published**: 30 Nov 2018

Abstract

Development of novel materials for an efficient harvesting of solar energy towards applications in environment and energy sectors is an important area of research. A metal-free polymeric material, g-C_3N_4 is modified with three Cu(I)-based oxides namely Cu_2O, $CuVO_3$, and Cu_3VO_4 to extend the absorption of the solar spectrum. The composite structures are synthesized by a facile one-step solid-state reaction under inter atmosphere and atmospheric pressure. The amounts of loadings of Cu(I)-based oxides onto g-C_3N_4 is varied from 2 wt.% to 10 wt.%. Powder XRD patterns showed that the graphitic structure of carbon nitride is maintained upon the construction of hybrid structures with Cu(I) oxides. SEM images show the textural transformation of the bulk structure of g-C_3N_4 into nanosheets upon thermal retreatment. FT-IR spectra further confirmed the stability of g-C_3N_4 observed in the XRD patterns. In comparison with the pristine g-C_3N_4, the DR-UV-Vis spectra of the modified solid powders demonstrated a clear red shift in the absorption towards higher wavelength and their better prospects in harvesting solar energy. Tauc plots derived from the DR-UV-Vis spectra showed a narrowing of the direct-allowed band gap upon modifications with Cu(I)-based oxides. The composites showed moderate activity in photocatalytic degradation of rhodamine B under irradiation from a solar simulator.

Keywords: Cu(I)-based Oxides, g-C_3N_4, Composites, Visible-active, Photocatalysis

Introduction

Photocatalysis is an important area of research to combat with the environmental challenges and for the production of renewable energy and chemicals. A polymeric metal-free semiconductor, graphitic carbon nitride (g-C_3N_4) has quickly turn out to be an important material in photocatalysis [1-3]. Research on the development of photocatalysts materials, mainly TiO_2 began with the findings of Fujishima and Honda in 1972 [4]. Lately, polymeric semiconductor g-C_3N_4 is getting increased attention as a photocatalyst material. Since the first reports in 2009, this metal-free semiconductor, g-C_3N_4 has been attracting enormous attention [5]. The bulk, pale yellow color g-C_3N_4 is a p-type semiconductor with band gap size of ~2.7 eV. For the highly desired photocatalytic water splitting and H_2 generation reaction, the valence and conduction band gap positions of g-C_3N_4 sandwich both oxygen and hydrogen evolution potentials, making it an important material for further investigations. However, separation of photoexcited electron-hole pairs is an intrinsic problem with g-C_3N_4 and an active area of research on its modifications [1,2]. Furthermore, the position for absorption of visible light is just on the borderline with UV light. Therefore, the coupling of g-C_3N_4 with other suitable semiconductors is important for efficient separation of electron-hole pairs and for harvesting a wider spectrum of solar energy [1,2].

Doping, dye-sensitization, and fabrication of heterostructures are the main approaches for extending absorption and enhancing the separation of electron-hole pairs [3]. Moreover, bandgap engineering of g-C_3N_4 with suitable plasmonic materials also helps in photocatalysis. Here in this study, we are investigating on g-C_3N_4 combinations with Cu(I)-based oxides for the fabrication of efficient and stable photocatalyst systems. Cu(I)-based materials have important applications in catalysis and in harvesting solar energy [6,7]. The simplest Cu(I) oxide, Cu_2O recently attracted attention due to its non-toxic nature, low-cost, abundance and simple fabrication process [8]. However, Cu(I) oxidation state is prone to both oxidation and reduction under the applied conditions. Therefore, various approaches have been applied to preserve the Cu(I) state. Synthesis of multimetal oxides of Cu(I) is one of the important strategies in gaining stability of the species [9,10]. Modifications of g-C_3N_4 with Cu_2O have been reported for photocatalytic applications [11-15]. Besides, a core-shell structure of Cu_2O and g-C_3N_4 is active as a sensor material [16]. Some ternary composites including Cu_2O and g-C_3N_4 have also been investigated [17-20]. Mainly, fabrications of Cu_2O/g-C_3N_4 heterojunctions were carried out in a number of steps, via a chemical reduction of Cu(II) on g-C_3N_4.

Stability of Cu(I) oxidation state under the working conditions is a serious issue, as Cu(I) oxide is easily reduced to Cu(0) metal or get oxidized to Cu(II) oxide, and all the three oxidation state (0, I, II) may co-exist in a ternary composite; Cu-Cu_2O-CuO [19]. In order

to overcome the instability of cuprous oxide, it has been mixed with other metal oxides to increase the strength of the Cu-O bond [7,10]. Among all the Cu(I)-based multimetal oxides with Group-V metals, especially, novel properties of $CuVO_3$ makes it a potential semiconductor in solar cell applications [10]. Furthermore, $CuVO_3$ has high-intensity resonant bands in the visible range, with a broad absorption edge compared to the other two materials. Solid-state synthesis of semiconducting compounds of Cu(I) and Group-V oxides; $CuVO_3$, $CuNbO_3$, and $Cu_5Ta_{11}O_{30}$ were reported earlier [10]. The temperature for the synthesis of $CuVO_3$ is the lowest (550 °C) and suitable for its in-situ synthesis and fabrication of heterojunction with g-C_3N_4 [10,21,22]. On the other hand, high-temperature requirements for the synthesis of $CuNbO_3$ and $Cu_5Ta_{11}O_{30}$ at 900 °C and 1100 °C, respectively, are unsuitable for their in-situ growth on g-C_3N_4 [10]. Another semiconductor of Cu(I) vanadate with an increased ratio of copper, Cu_3VO_4 is synthesized at around 550 °C, making it suitable for fabrication of heterojunction with g-C_3N_4 [23,24]. V_2O_5 is also hybridized with g-C_3N_4 for interesting visible light driven photocatalytic properties [25]. However, no reports exist on the g-C_3N_4 modifications with Cu(I)-based multimetal oxides with vanadium ($CuVO_3$, and Cu_3VO_4). In an effort to make visible-light active photocatalyst systems, we investigated on a facile one-step solid-state fabrication of g-C_3N_4 composites with various Cu(I)-based oxides; Cu_2O, $CuVO_3$, and Cu_3VO_4.

Materials and Methods

Reagent grade melamine ($C_3H_6N_6$; 99%, Aldrich), Cu_2O (98%; Aldrich), and V_2O_5 (99.2%; Alfa Aesar) as-received from the manufacturers are used for the synthesis of composite photocatalyst materials. An aqueous phase of rhodamine B (99%; Acros) is used as a model organic pollutant for the photocatalytic degradation studies.

Synthesis of materials

Pure phase bulk g-C_3N_4 is synthesized from thermal treatment of melamine powder under static air in an alumina crucible with a cover. Solid-state reactions were carried out at different temperatures and an optimized reaction condition is, 550 °C for 4 h. Yellow powder product, g-C_3N_4 is received upon thermal treatment of melamine. Thermal etching of bulk g-C_3N_4 into its nanosheet structure is carried out under Ar flow at 550 °C, 2 h for comparing with hybrid structures of Cu(I)-based oxide(s) and g-C_3N_4.

For the synthesis of composite materials, as-prepared bulk g-C_3N_4 is thoroughly mixed with an appropriate amount of Cu(I)-based semiconductor precursor(s). Thus prepared physical mixture is taken in an alumina boat and closed in a reactor connected with argon gas. The reactor system is placed in the muffle furnace and heated to the required temperature under inert atmosphere. Thermal treatment of bulk g-C_3N_4 has been reported for its conversion into nanosheets. Therefore, as a control, bulk g-C_3N_4 in the absence of Cu(I)-based oxides is also heated under same inert conditions.

(1) Cu_2O/g-C_3N_4: For the solid-state synthesis of a heterojunction of simple Cu(I) oxide, Cu_2O and g-C_3N_4, the precursors are homogenized in a mortar with a pestle. A red-brown commercial sample of Cu_2O is mixed well with an as-prepared yellow sample of bulk g-C_3N_4. The concentration of Cu_2O loaded onto g-C_3N_4 is varied from 2 wt.% to 10 wt.%. A mixture of precursors is taken in an alumina boat and thermally treated under flowing Ar to construct a heterojunction between Cu_2O and g-C_3N_4. The physical mixture is heated in a muffle furnace to the reaction temperature ranging from 200 °C to 550 °C for 2 h using a ramping rate of 4 °C min^{-1}. By the end of the solid-state reaction, the reactor is naturally cooled yet under flowing Ar gas. Once the temperature is normalized to room temperature the product is taken out and ground to a fine powder for further use.

(2) $CuVO_3$/g-C_3N_4: Solid-state synthesis of pure phase $CuVO_3$ from a 1:1 molar mixture of Cu_2O and V_2O_5 is carried out following a report study [10]. For the construction of a heterojunction of $CuVO_3$ and g-C_3N_4, the precursors are homogenized in a mortar with a pestle. Required molar concentrations of a red-brown sample of Cu_2O and a yellow sample of V_2O_5 are mixed well with an as-prepared yellow sample of bulk g-C_3N_4. For the composite, $CuVO_3$/g-C_3N_4, a physical mixture of precursors is taken in an alumina boat and thermally treated under flowing Ar gas. All the samples with various concentrations of 2 wt.% to 10 wt.%. $CuVO_3$ loaded onto g-C_3N_4 are heated in a muffle at 550 °C for 2 h using a ramping rate of 4 °C min^{-1}. The flow of Ar gas is continued during natural cooling of the reactor. By the end, the product is taken out and ground to a fine powder for further use.

(3) Cu_3VO_4/g-C_3N_4: Solid-state synthesis of pure phase Cu_3VO_4 from a 3:1 molar mixture of Cu_2O and V_2O_5 is carried out following a report study [24]. For the construction of a heterojunction of Cu_3VO_4 and g-C_3N_4, the precursors are homogenized in a mortar with a pestle. Required molar concentrations of a red-brown sample of Cu_2O and a yellow sample of V_2O_5 are mixed well with an as-prepared yellow sample of bulk g-C_3N_4. For the composite, Cu_3VO_4/g-C_3N_4, a physical mixture of precursors is taken in an alumina boat and thermally treated under flowing Ar gas. All the samples with various concentrations of 2 wt.% to 10 wt.%. Cu_3VO_4 loaded onto g-C_3N_4 are heated in a muffle at 550 °C for 2 h using a ramping rate of 4 °C min^{-1}. The flow of Ar gas is continued during natural cooling of the reactor. By the end, the product is taken out and ground to a fine powder for further use.

Characterization

X-ray diffraction (XRD) patterns for powder samples are recorded on a Rigaku diffractometer, model MiniFlex operating at 40 kV and 50 mA. XRD patterns in the 2-theta range of 5–80 degree are recorded using Cu Kα radiation. Scanning electron microscopy (SEM) analyses g-C_3N_4 and composite samples are performed to study the changes in the textural properties. Powder samples are spread on a carbon tape pasted onto an aluminum alloy mounts and observed under the microscope. Images are recorded on a high-performance Hitachi S-3400N microscope. Fourier transformed infrared (FT-IR) spectra are measured on a Bruker spectrometer, model Vector 22. IR spectra of powder samples are measured with attenuated total reflectance (ATR) mode. Optical spectra are recorded on a UV–Vis spectrophotometer (Shimadzu, model UV-3600) with a diffuse reflectance (DR) attachment. Powder material is pressed in a sample holder and DR-UV-Vis spectra are recorded in the range of 220–800 nm.

Photocatalytic Testing

Photocatalytic degradation of rhodamine B is examined in a glass beaker with a solar simulator light shining from the top. 100 mg of catalyst powder is suspended in water and mixed with an adequate concentration of rhodamine B. Total volume of aqueous solution is 100 ml and it is stirred with a bar magnet at 300 rpm under dark for 30 min. A small aliquot of the mixture is taken out to assess the

dye sorption on solid powder. Then the reaction mixture is exposed to light from the solar simulator, adjusted to 1 sun illumination. At regular intervals, samples are drawn from the reaction mixture to examine the photodegradation of organic dye. The reaction mixtures are centrifuged for separating solid and liquid phases. The amount of rhodamine B in the aqueous phase is optically analyzed on a Cary UV-Vis spectrophotometer, model 100 Bio.

Results and Discussion

Physicochemical Properties

The graphitic g-C_3N_4 structure is maintained in all the pure and modified samples as indicated by diffraction patterns and supported with FT-IR and DR-UV-Vis spectra. The bulk g-C_3N_4 is synthesized from the solid-state conversion of melamine at 550 °C (Figure 1a). Two characteristics diffraction peaks (100) and (002) for the pure g-C_3N_4 appeared around 2-theta position of 13.1o and 27.6o (Figure 1). The main XRD peak at 27.6o is due to graphite-like stacking of the C_3N_4 layers [26]. Before analyzing the physicochemical properties of g-C_3N_4 modified with Cu(I)-based oxides it is important to understand any changes in the lonely g-C_3N_4 under the reaction conditions. XRD patterns and FT-IR spectra of bulk g-C_3N_4 and after its thermal treatment under Ar flow at 550 °C for 2 h are presented in Figure 1. The main (002) diffraction peak of the bulk g-C_3N_4 decreased more than 50% upon thermal re-treatment indicating the conversion of bulk into more like nanosheet structure. FT-IR spectra also demonstrated clear changes in the intensity upon transformation of bulk g-C_3N_4 into nanosheets. In contrast to a decreased intensity of diffraction peaks, an enhancement in the all the vibrational stretching is observed for the nanosheet structure of g-C_3N_4. These changes in the physicochemical properties of upon conversion of bulk g-C_3N_4 into nanosheets are a reference point when describing results of the composite materials.

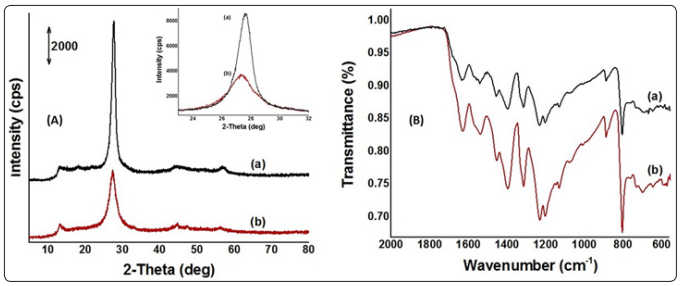

Figure 1: (A) XRD patterns, and (B) FT-IR spectra of bulk g-C_3N_4 (a) and after its thermal treatment under Ar flow at 550 °C, 2 h for conversion into nanosheets (b).

Representative SEM images of bulk g-C_3N_4 and after its thermal retreatment for textural conversion into nanosheets are shown in Figure 2. SEM image of bulk g-C_3N_4 exhibited irregular and inter-grown large particles (Figure 2A). Thermal treatment of bulk g-C_3N_4 has been reported for its textural conversion into nanosheet structure [27],[28]. Figure 2B depicts an SEM image of thermally treated bulk g-C_3N_4, and after its conversion into the flake-like structure. These visual changes observed in the SEM images further confirmed the thermal transformation of the bulk structure into nanosheets as examined in the XRD and FT-IR investigations.

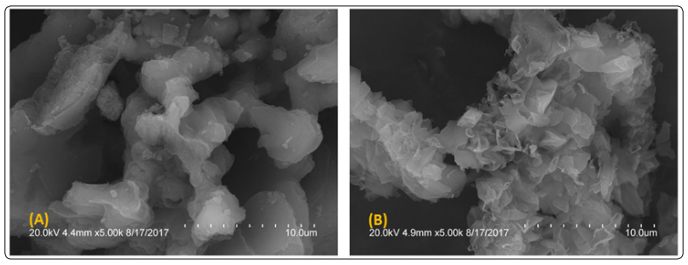

Figure 2: SEM images of (A) bulk g-C_3N_4, and (B) after its thermal treatment under Ar flow at 550 °C, 2 h for conversion into nanosheets.

XRD patterns of pristine g-C_3N_4 with 0% to 10% Cu+Cu_2O mixtures thermally treated under inert conditions are shown in Figure 3. As demonstrated by the XRD patterns in Figure 3A, the graphitic structure is maintained under the reaction conditions. For a low amount (2% Cu+Cu_2O) mixture with g-C_3N_4, no visible diffraction peaks are seen for the metal/metal oxide(s). With an increased loading (5% Cu+Cu_2O), small diffraction peak features appeared beyond 40 degrees. Further enhanced diffraction peaks are noticed in the 10% Cu_2O and the g-C_3N_4 mixture heated under Ar flow. Cu(I) state is unstable and prone to various redox behaviors and co-existence of multiple states under the applied reaction conditions. Inert conditions of this solid-state reaction conditions led to a partial reduction of Cu_2O to metallic Cu as seen in the XRD patterns. Reduction of Cu(I) to metallic copper, Cu(0) has been reported in the earlier studies on the construction of heterojunctions [13,20]. In the case of the Cu_2O/g-C_3N_4 composite structure containing metal oxide as a major component, essentially, no crystalline graphitic carbon nitride signature peaks are seen in the XRD patterns [15]. In the previous studies, hybrid structures of Cu_2O with g-C_3N_4 were prepared mainly via a chemical reduction process of Cu(II) precursor [11-13,20,29]. Furthermore, various ternary composites have been investigated to gain enhanced stability of the catalyst material, Cu_2O/g-C_3N_4, and separation of photoexcited electron-hole pairs [17,30].

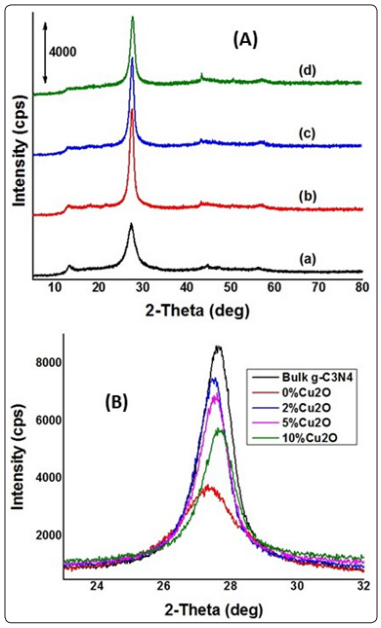

Figure 3: (A) XRD patterns and (B) main (002) diffraction peak of pure g-C_3N_4 (a), and its mixture with 2% Cu_2O (b), 5% Cu_2O (c), and 10% Cu_2O thermally treated under Ar flow at 550 °C, 2 h.

In the absence of Cu_2O, bulk g-C_3N_4 clearly showed a transformation into the nanosheet structure as observed from a drastic decrease in the (002) peak intensity (Figure 3B). This decrease of the main peak intensity may come from the decreased stacking of sheets as noted in the case of thermal treatment of pure g-C_3N_4. In addition, a decrease in the main peak intensity is noted in the hybridized materials. For all the various mixtures of bulk g-C_3N_4 and Cu_2O treated under an inert atmosphere, the decrease in (002) peak intensity is not pronounced as it is observed for the pure g-C_3N_4 the (Figure 3B). The main peak intensity of main diffraction peak of g-C_3N_4 is decreasing with increased loading of $CuVO_3$ but it is never lower than the intensity level achieved in the absence of the multimetal oxide whereupon the bulk structure is converted into nanosheets. Hence, the presence of metal oxide decreases the conversion of bulk g-C_3N_4 into nanosheets. A sequential decrease in the intensity of (002) diffraction peak of g-C_3N_4 upon increasing the Cu+Cu_2O loading from 2% to 10% may originate for the composite structures with a limited delamination of graphitic sheets. A sequential decrease in the peak intensity of graphitic structure has been recorded with an increased loading of Cu_2O+Cu [13,20]. In addition to the reaction conditions for the formation of Cu_2O, the concentration of its precursor was found important in controlling oxidation state of copper.

Structural studies of g-C_3N_4 modified with 0% to 10% $CuVO_3$ prepared from thermal treatment of 1:1 mixture of Cu_2O:V_2O_5 under inert conditions are shown in Figure 4.

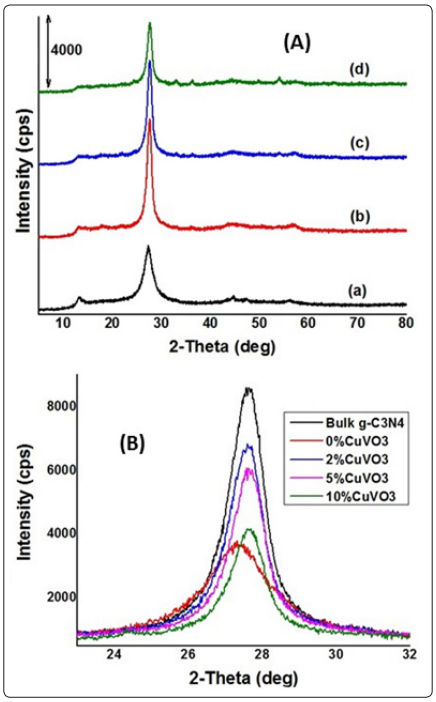

Figure 4: (A) XRD patterns and (B) main (002) diffraction peak of pure g-C_3N_4 (a), and its mixture with various amounts of Cu_2O+V_2O_5 (1:1) corresponding to; 2% $CuVO_3$ (b), 5% $CuVO_3$ (c), and 10% $CuVO_3$ (d) thermally treated under Ar flow at 550 °C, 2 h.

Similar to the heat treatment of the g-C_3N_4 mixtures with plain Cu_2O, XRD patterns showed that the graphitic structure is maintained during the formation of composites with multimetal oxide ($CuVO_3$) under Ar flow (Figure 4A). For g-C_3N_4 hybridized with 2% $CuVO_3$, diffraction peaks from the multimetal oxide are hardly visible in the pattern. Upon increasing the loading to 5%, some specific diffraction peaks for $CuVO_3$ appeared in the hybrid material, mainly in between 30–40 degrees. So, both g-C_3N_4 and $CuVO_3$ are keeping their structures upon the construction of heterojunction. Next, a further increase in the loading of $CuVO_3$ to 10% demonstrated clear peaks in the composite material. Interestingly, no XRD peaks from the reduction to metallic Cu are seen for the 1:1 mixture of Cu_2O:V_2O_5 and g-C_3N_4 heated under an inert atmosphere. On the other hand, clear diffraction peaks of metallic Cu are observed in the case of plain Cu_2O heated in the presence of g-C_3N_4, under Ar flow (Figure 3A). Hence, Cu_2O preferentially reacted with V_2O_5 towards the formation of $CuVO_3$ and remained stable as Cu(I) in the multimetal oxide. While a partial reduction of Cu(I) oxidation state to Cu(0) is observed when heating a mixture of Cu_2O and g-C_3N_4. This gain in thermal stability of Cu(I) oxidation state under inert conditions for the composite of multimetal oxide ($CuVO_3$) and g-C_3N_4 may be interesting in its catalytic applications.

Thermal treatment of bulk g-C_3N_4 under an inert atmosphere in the absence of any metal oxide(s), clearly showed a transformation into nanosheets, with a low regularity of the layered structure (Figure 2A). A decrease in the main diffraction peak intensity of g-C_3N_4 in the composite may come from its decreased concentration. Essentially, even a small concentration of metal(s) and the oxide(s) that are heavy compared with the nonmetallic base material, g-C_3N_4 may have a severe impact in denting the intensity of the main diffraction peak. As shown in Figure 4B, the composites of $CuVO_3$/g-C_3N_4 showed a similar trend of (002) diffraction as it is observed in the case of Cu+Cu_2O/g-C_3N_4 (Figure 3B). For the same level of metal oxide(s) loading e. g. 10% of $CuVO_3$ or Cu+Cu_2O, g-C_3N_4 composite with the former showed an understandably enhanced reduction in the (002) intensity. Therefore, parallel to the observations for the composite with Cu+Cu_2O, the presence of multimetal oxide decrease the conversion of bulk g-C_3N_4 into nanosheets.

Powder XRD patterns of pure g-C_3N_4 and its mixture with various amounts of Cu_2O+V_2O_5 (3:1) corresponding to loadings of 2% to 10% of Cu_3VO_4 by thermal treatment under Ar flow are presented in Figure 5. Similar to the other composites i. e. Cu+Cu_2O/g-C_3N_4 and $CuVO_3$/g-C_3N_4, X-ray studies of g-C_3N_4 hybrids with Cu_3VO_4 showed that the graphitic structure is maintained during the formation of composites (Figure 5A). For g-C_3N_4 composite with 2% Cu_3VO_4, diffraction peaks from the multimetal oxide are not seen in the pattern. However, with an increase of Cu_3VO_4 from 2% to 5%, specific diffraction peak features started to appear in the XRD pattern. A further increase of Cu_3VO_4 to 10% demonstrated clear diffraction peaks of the multimetal oxide in the composite material. Thus, similar to other Cu(I)-based hybrids, both g-C_3N_4, and Cu_3VO_4 are keeping their crystalline structures upon the construction of heterojunction. Interestingly, similar to $CuVO_3$/g-C_3N_4, no reduction of Cu(I) to metallic Cu is observed in the XRD pattern even for a 3:1 mixture of Cu_2O:V_2O_5 and g-C_3N_4 heated under an inert atmosphere. On the contrary, the formation of metallic Cu is observed in the case of plain Cu_2O heated with g-C_3N_4 under Ar flow (Figure 3A). Hence, Cu_2O preferentially reacted with V_2O_5 towards the formation of multimetal oxides, $CuVO_3$ and Cu_3VO_4, and remained stable as Cu(I). On the other hand, the oxidation state of Cu(I) is lowered to Cu(0) in the case the thermal treatment of a mixture of Cu_2O and g-C_3N_4. This gain in thermal stability of Cu(I) state under inert conditions for the composite of Cu_3VO_4 (and $CuVO_3$) with g-C_3N_4 may be interesting in its catalytic applications.

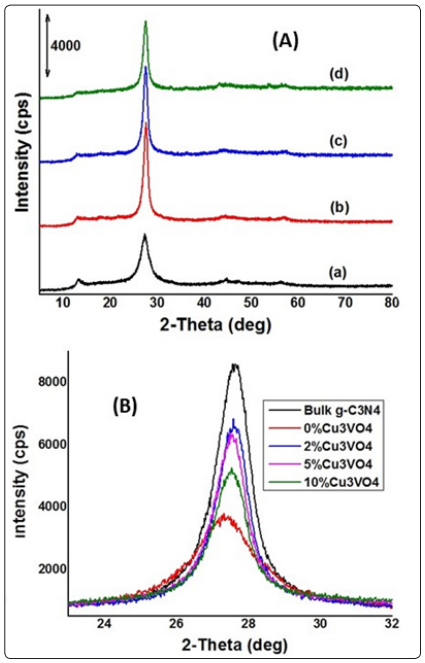

Figure 5: (A) XRD patterns and (B) main (002) diffraction peak of pure g-C_3N_4 (a), and its mixture with various amounts of Cu_2O+V_2O_5 (3:1) corresponding to; 2% Cu_3VO_4 (b), 5% Cu_3VO_4 (c), and 10% Cu_3VO_4 (d) thermally treated under Ar flow at 550 °C, 2 h.

As discussed above, the thermal treatment of bulk g-C_3N_4 under inert atmosphere transformed the bulk material into nanosheets (Figure 1A). Additionally, a decrease in the main diffraction peak intensity of g-C_3N_4 in the composite materials may come from its decreased concentration as demonstrated for $CuVO_3$/g-C_3N_4. A similar behavior of (002) diffraction is observed for the Cu_3VO_4/g-C_3N_4 composite, as shown in Figure 5B. In conclusion, during the thermal heating of g-C_3N_4 under inert atmosphere its extensive conversion to nanosheets is realized when pure, but, decreased by the presence of plain Cu_2O or Cu_2O+V_2O_5 mixtures.

The vibrational spectra of the pristine g-C_3N_4 and its mixtures with Cu_2O alone or mixtures of Cu_2O+V_2O_5 thermally treated under Ar flow are presented in Figure 6. FT-IR spectra for the bulk g-C_3N_4 and upon its thermal conversion into nanosheets is shown in Figure 1B with a clear enhancement of the intensity of IR active bands. Prominent signatures of IR sensitive functional groups are seen in the range of 1700 cm^{-1} to 700 cm^{-1}. The presence of IR bands around 1635 cm^{-1} and 1240 cm^{-1} is illustrating stretching vibrations of C=N and C–N groups, respectively. For the s-triazine ring mode, a sharp band appeared at 805 cm^{-1} along with a low-intensity feature around 1465 cm^{-1}. The g-C_3N_4 modified with Cu(I)-based oxides by an in-situ method essentially maintained its functionalities as demonstrated by FT-IR spectra in Figure 6. The intensity of IR bands of g-C_3N_4 showed a relative decrease after all the modifications with semiconductor oxides and confirm the decreased formation of nanosheets. In comparing with the pure material, a change in the environment for the modified g-C_3N_4 caused a smaller difference in electronegativity of CN groups, hence decreased the strength of IR bands. Importantly, the strength of IR bands showed a sequential decrease against an increase in the concentration of Cu(I)-based oxides in the composites structures.

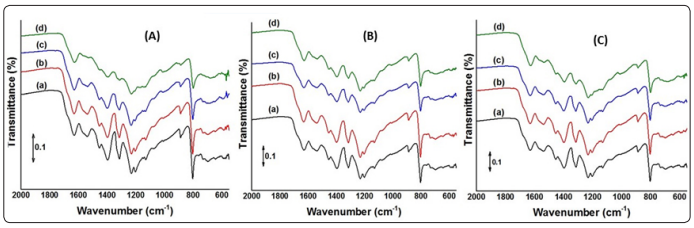

Figure 6: FT-IR spectra of pure g-C_3N_4 (a) and its mixture with; (A) 2% Cu_2O (b), 5% Cu_2O (c), 10% Cu_2O (d), (B) various amounts of Cu_2O+V_2O_5 (1:1) corresponding to; 2% $CuVO_3$ (b), 5% $CuVO_3$ (c), and 10% $CuVO_3$ (d), and (C) various amounts of Cu_2O+V_2O_5 (3:1) corresponding to; 2% Cu_3VO_4 (b), 5% Cu_3VO_4 (c), and 10% Cu_3VO_4 (d) thermally treated under Ar flow at 550 °C, 2 h.

The optical spectra for pure g-C_3N_4 and after its modification with a mixture of Cu+Cu_2O are shown in Figure 7A. The absorption edge for g-C_3N_4 is laying at around 460 nm and further confirmed on the purity of g-C_3N_4 characterized by XRD and FT-IR. After g-C_3N_4 modifications with cuprous oxide, the main features of optical spectra are similar to those of the pure material. However, the absorption edge is shifted towards higher wavelength demonstrating an enhanced absorbance of the visible light. In addition to a red-shift of the optical spectra for the hybridized material, the baseline also shifted upwards indicating surface defects in the composites. Hence, the optical properties of the composites with Cu+Cu_2O demonstrated better prospects in photocatalysis under solar irradiation. Overall, modifications of g-C_3N_4 with cuprous oxide demonstrated an extended absorption of the solar spectrum. Tauc plots derived from the DR-UV-Vis spectra are shown in Figure 7B. Pristine g-C_3N_4 and modified materials are found with direct allowed bandgap type. The size of the bandgap is shrinking upon increased loading of Cu+Cu_2O in the hybrid semiconductor. For the pure g-C_3N_4, the bandgap size is around 2.79 eV (Table 1). The bandgap size decreased to 2.68 eV for the modified material, 2% Cu+Cu_2O/g-C_3N_4. With the increase of Cu+Cu_2O to 10%, the bandgap (2.34 eV) is further extended towards higher wavelength and found suitable for harvesting solar energy. As expected for hybridization of g-C_3N_4 with Cu_2O, previous studies have also reported on the monotonous shortening of the bandgap size of the composites with an increased loading of the later [11], [14].

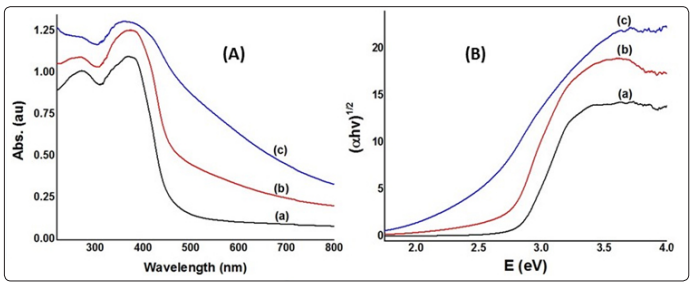

Figure 7: (A) Optical spectra and (B) Tauc plots of pure g-C_3N_4 (a) and its mixture with 2% Cu_2O (b), 10% Cu_2O (c) thermally treated under Ar flow at 550 °C, 2 h.

The solid-state DR-UV-Vis spectra of the pure g-C_3N_4 and after its hybridization with $CuVO_3$ are presented in Figure 8A. The absorption edge of g-C_3N_4 (460 nm) is shifted towards higher wavelength side after modifications with $CuVO_3$. A homogeneous structure of $CuVO_3$/g-C_3N_4 is illustrated from the optical spectra in Figure 8A, and further confirmed the purity of g-C_3N_4 characterized by XRD and FT-IR. After the modifications of g-C_3N_4 with $CuVO_3$, the main

features of optical spectra are similar to those of the pure material, the absorption edge is shifted towards higher wavelength demonstrating an enhanced absorbance of the visible light. A sequential increase in the concentration of 0% to 10% $CuVO_3$ loaded in the g-C_3N_4, the bandgap is sequentially narrowed down as depicted in Table 1. However, in addition to a red-shift in the optical spectra of the hybridized material, the baseline is also shifted upwards indicating surface defects in the composites. Hence, the optical properties of the composites with $CuVO_3$ demonstrated better prospects in photocatalysis under solar irradiation. Overall, modifications of g-C_3N_4 demonstrated an extended absorption of the solar spectrum. Tauc plots derived from the DR-UV-Vis spectra demonstrated direct allowed bandgap type for $CuVO_3$/g-C_3N_4 (Figure 8B). The size of the bandgap is narrowed upon increased loading of $CuVO_3$ in the hybrid semiconductor. The bandgap size of pure g-C_3N_4 (2.79 eV) is decreased to 2.74 eV upon modification with 2% $CuVO_3$. Similar to the observations for the various loadings of Cu+Cu_2O (2% to 10%), sequentially, the bandgap decreased from 2.68 eV (5% $CuVO_3$) to 2.59 eV (10% $CuVO_3$) with further extending the g-C_3N_4 absorption towards higher wavelength for harvesting solar energy. In comparison with bare Cu_2O (2.0 eV), a considerably shrinking of the optical bandgap size has been reported for the multimetal oxide, $CuVO_3$ (1.4 eV) from both the experimental and computational investigations [7,10]. Hence, the fabrication of heterojunctions of $CuVO_3$ with g-C_3N_4 illustrated a systematic decrease of the bandgap size with an increased loading of the multimetal oxide (Table 1).

Table 1: Bandgap size of g-C_3N_4 and afters its modifications with various Cu(I)-based semiconductors determined from Tauc plots derived from optical spectra

#	Material	Band gap† (eV)
1	Pure g-C_3N_4	2.79
2	2%Cu+Cu_2O/g-C_3N_4	2.68
3	10%Cu+Cu_2O/g-C_3N_4	2.34
4	2%$CuVO_3$/g-C_3N_4	2.74
5	5%$CuVO_3$/g-C_3N_4	2.68
6	10%$CuVO_3$/g-C_3N_4	2.59
7	2%Cu_3VO_4/g-C_3N_4	2.71
8	5%Cu_3VO_4/g-C_3N_4	2.64
9	10%Cu_3VO_4/g-C_3N_4	2.51

†The band gap determined from Tacu plot is the direct allowed type.

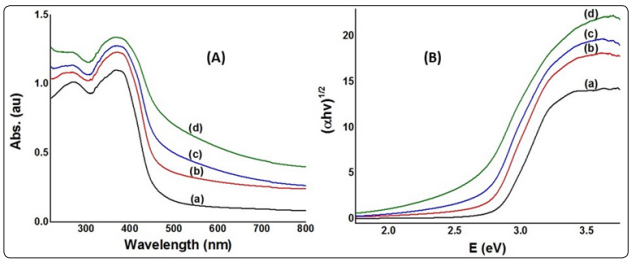

Figure 8: (A) Optical spectra, and (B) Tauc plots of pure g-C_3N_4 (a) and its mixture with various amounts of Cu_2O+V_2O_5 (1:1) corresponding to; 2% $CuVO_3$ (b), 5% $CuVO_3$ (c), and 10% $CuVO_3$ (d) thermally treated under Ar flow at 550 °C, 2 h.

The optical spectra of g-C_3N_4 powder modified with Cu_3VO_4 are shown in Figure 9A. Similar to the behaviors of Cu+Cu_2O and $CuVO_3$ modified g-C_3N_4 samples, the absorption edge (460 nm) is shifted towards higher wavelength side after modifications with Cu_3VO_4. A homogeneous structure of Cu_3VO_4/g-C_3N_4 is illustrated from the optical spectra in Figure 9A, and further confirmed characterizations by other techniques. After g-C_3N_4 modifications with Cu_3VO_4, the main features of optical spectra are similar to that of the pure material, the absorption edge is shifted towards higher wavelength demonstrating an enhanced absorbance of the visible light. For a sequential increase in the Cu_3VO_4 concentration from 0% to 10% loaded in the g-C_3N_4, the bandgap size is shrinking as depicted in Table 1. However, in addition to a red-shift of the optical spectra for the hybridized material, the baseline also shifted upwards indicating surface defects in the composites. Hence, the optical properties of the composites with Cu_3VO_4 demonstrated favorable properties in harvesting solar irradiation. Both, pristine g-C_3N_4 and Cu_3VO_4 modified materials are found having a direct allowed bandgap type as determined from Tauc plots of the DR-UV-Vis spectra (Figure 9B). The size of the bandgap is narrowing down upon increased loading of Cu_3VO_4 in the hybrid semiconductors. Similar to the modifications with Cu+Cu_2O and $CuVO_3$, the bandgap size is decreased from 2.79 eV for 0% Cu_3VO_4 to 2.51 eV upon modification with 10% Cu_3VO_4, thus, extending the absorption towards higher wavelength for harvesting solar energy. A monotonous widening of the absorption spectrum of Cu_3VO_4/g-C_3N_4 composites towards the visible side, with an increased loading of the multimetal oxide, is attributed to its small optical bandgap size, 1.2 eV [7,24].

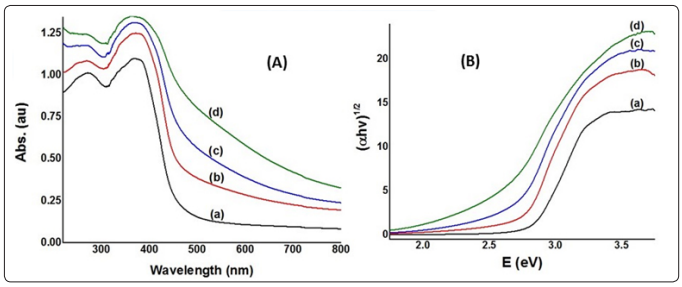

Figure 9: (A) Optical spectra, and (B) Tauc plots of pure g-C_3N_4 (a) and its mixture with various amounts of Cu_2O+V_2O_5 (3:1) corresponding to; 2% Cu_3VO_4 (b), 5% Cu_3VO_4 (c), and 10% Cu_3VO_4 (d) thermally treated under Ar flow at 550 °C, 2 h.

Photocatalytic Efficiency

Photocatalytic properties are tested for the degradation of rhodamine B in the aqueous phase. For the dye stability check, rhodamine B solution of the same concentration as mixed with photocatalysts is exposed to light from the solar simulator, 1 sun illumination. Essentially, no photolysis of rhodamine B is observed under the experimental conditions. Before exposing the suspension to the light, sorption of dye on the powder catalyst is equilibrated by stirring under dark. A small aliquot is taken out every 30 min to quantify the amount of dye in the liquid phase. Before recording the UV-Vis spectra, liquid, and solid phases are separated by centrifuge. Under dark, no appreciable decrease in rhodamine B is noticed for any of the materials applied in this study (Figure 10). After equilibrating the dye adsorption for 30 min, the suspension is exposed to the light from a solar simulator operating at 1 sun illumination. Upon shining light, a decrease in the dye concentration is observed for all the materials demonstrating their photocatalytic activity. Loading of a moderate amount of Cu_2O (~1.5 wt.%) on g-C_3N_4 has been reported for an enhanced photocatalytic activity [11]. Therefore, here in this study, the composites of Cu(I)-based oxides/g-C_3N_4

loaded with a similar amount of metal oxide(s) (2 wt.%) are used in the photocatalytic activity tests.

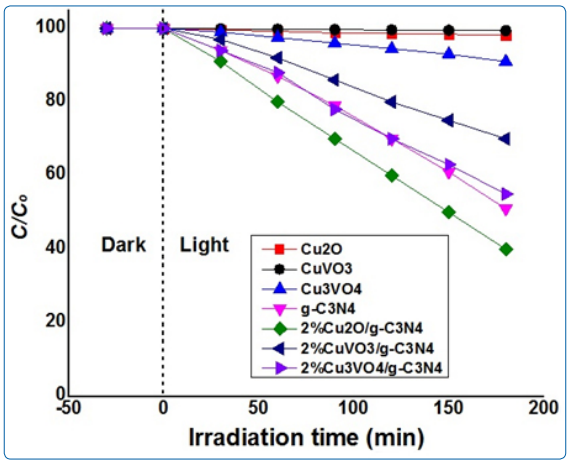

Figure 10: Solar light-driven photodegradation of aqueous phase rhodamine B over all the various semiconductor catalyst materials.

As shown in Figure 10, pure Cu_2O and $CuVO_3$ are almost inactive for the photodegradation of rhodamine B under the experimental conditions. Cu_3VO_4 depicted a slight efficiency with about 9% photodegradation of the dye upon solar light irradiation for 180 min. In comparison with a low activity of pure phase Cu(I)-based oxides, unmodified g-C_3N_4 demonstrated a moderate photocatalytic activity. For the same time (180 min) of irradiation with simulated solar light, then about 49% of rhodamine B is decomposed over this polymeric semiconductor, g-C_3N_4. Photocatalytic tests over all the composites of g-C_3N_4 with 2% to 10% of various Cu(I)-based oxides are performed under 1 sun illumination. Among all the composites, a low concentration (2%) of Cu(I) oxide semiconductor is found more active for photodegradation of rhodamine B. Therefore, photocatalytic results only for the best composite materials are shown in Figure 10. Composites of g-C_3N_4 with multimetal oxide des ($CuVO_3$ and Cu_3VO_4) are relatively less active compared with simple oxide (Cu_2O). 2% $CuVO_3$/g-C_3N_4 showed the least activity among all the composites, with only about 30% photodegradation of rhodamine B in 180 min. Next, 2% Cu_3VO_4/g-C_3N_4 demonstrated a moderate photocatalytic activity and about 45% of the organic dye is decomposed up, on solar light irradiation for 180 min. The best photocatalytic performance is realized over 2% Cu+Cu_2O/g-C_3N_4. About 60% of rhodamine B is destroyed under the experimental conditions. Importantly, the catalyst materials remained stable under the experimental situation and showed steady performance in repeated runs. Hence, fabrication of heterojunction of Cu(I)-based oxide with g-C_3N_4 is effective in harvesting solar energy for the photodegradation of environmental pollutant.

Important to note that the Cu_2O/g-C_3N_4 composite contacting metallic Cu species is helpful for the separation of photoexcited charges and demonstrated the best photocatalytic activity among all the materials employed in this study. An enhanced photoactivity of a hydrothermally synthesized composite of Cu_2O/g-C_3N_4 having a presence of reduced metal component has been reported for the degradation of organic pollutant [13]. Essentially, all the composites of Cu(I)-based oxides/g-C3N4 are effective towards harvesting visible light from the solar spectrum, however, Cu_2O/g-C_3N_4 with Cu(0) exhibited an enhanced photocatalytic efficiency because of improved separation of photoexcited charges. Therefore, further modifications of the composites for an effective separation of photogenerated electron-hole pairs may strengthen the scope of their applications in environment and energy sectors.

In the reported studies, Cu_2O/g-C_3N_4 based composite structures have been tested for the photocatalytic evolution of hydrogen from water splitting, oxidation of CO, and degradation of organic pollutants [11-15,17,20,29,30]. In comparison with individual components, a ternary composite, Cu_2O-TiO_2/g-C_3N_4 exhibited a high photocatalytic efficiency for discoloration of organic dyes in the presence of hydrogen peroxide [17]. Photocatalytic oxidation of CO was attributed to a synergetic effect between g-C_3N_4 and Cu_2O with an improved dispersion of the metal oxide particles [29]. For all the various composites reported for Cu_2O and g-C_3N_4, an overall enhancement of the photocatalytic efficiencies have been demonstrated compared with bare semiconductors. In addition to the positive impact of heterojunction formation between Cu_2O and g-C_3N_4, the formation of metallic Cu species was found favorable for the separation of charges and consequently exhibiting improved photocatalytic properties [13]. Furthermore, the presence of reduced graphene oxide in the composite structure of Cu_2O/g-C_3N_4 facilitated the charge separation and efficiency towards the photocatalytic reaction [30]. In addition to the efficient photocatalytic properties of g-C_3N_4 heterojunctions with Cu_2O, its composite with V_2O_5 has been reported for enhanced photodegradation of rhodamine B under visible light [25].

A schematic of the efficient harvesting of solar energy for the composites compared with bare g-C_3N_4 is illustrated in Figure 11. In principle, the fabrication of a heterojunction of semiconductors is beneficial towards an enhanced separation of photoexcited electron-hole pairs. The optical properties clearly demonstrate a red-shift with an enhanced absorption of visible-light of the solar spectrum. The concentration of Cu(I)-based semiconductors is the guiding factor in making these composites suitable and efficient for harvesting solar energy. As shown the schematic, transfer of electrons and holes in between two semiconductors of a heterojunction helps in avoiding their recombination (Figure 11). Therefore, a suitable pair of semiconductor materials joined in a heterojunction are indeed making together an efficient photocatalytic system. Beside electronic properties, the transformation of textural properties may positively impact the photocatalytic activity of the composite. Essentially, the photocatalytic efficiency is increased with an increased availability of photoexcited electrons and holes at conduction band and valence band, respectively. Furthermore, in comparison with its individual components, a composite structure may gain stability against the most prone photocorrosion reaction on the surface of the materials, under the experimental conditions. Overall, this approach of developing novel heterojunctions is leading towards practicable photocatalytic systems to combat the environmental and energy issues. Cu(I)-based heterojunctions with g-C_3N_4 fabricated via solid-state approach are potential candidates for various catalytic applications of harvesting solar energy.

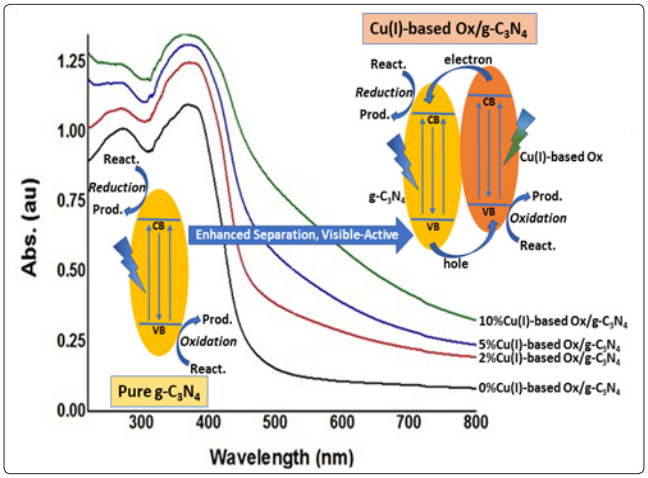

Figure 11: A schematic in the backdrop of optical spectra for the generation of photoexcited electron-hole pairs and their use at conduction band (CB) and valence band (VB) for photoreduction and photooxidation processes, respectively. In comparison with pure g-C_3N_4, an enhanced photoactivity and separation of electron-hole pairs is illustrated on the composite(s), Cu(I)-based oxide(s)/g-C3N4.

Conclusions

The composite structures of g-C_3N_4 with Cu(I)-based oxides are successfully fabricated via a facile solid-state route. An in-situ synthesis of multimetal Cu(I)-based oxides, $CuVO_3$ and Cu_3VO_4 along with their simultaneous composite formation with g-C_3N_4 are realized under inert conditions. In the presence of a second metal, the multimetal oxide of Cu(I)-based material helped in gaining stability of cuprous species in the composite structures. Hence, except for the reduction of Cu(I) observed in Cu_2O/g-C_3N_4, all the other composites ($CuVO_3$/g-C_3N_4 and Cu_3VO_4/g-C_3N_4) showed an enhanced stability of cuprous species. The physicochemical properties of the heterojunctions illustrated on the dispersion of the inorganic oxides onto g-C_3N_4. In contrast to the thermal conversion of the bulk pure g-C_3N_4 into nanosheets, the presence of Cu(I)-based oxides hindered the textural transformation. All the heterojunctions of inorganic-organic semiconductors demonstrated the direct allowed type of bandgap. Essentially, the bandgap size is narrowed down in all the composite, hence, making the modified materials suitable for harvesting solar energy. All the hybrid materials showed photodegradation of aqueous phase rhodamine B under the simulated solar light while pure Cu(I)-based oxides are mainly inactive. Further modifications are required for improving the separation of photoexcited electron-hole pairs, and consequently enhancing the photoactivity.

Acknowledgment

This research work was financially supported by the Natural Sciences and Engineering Research Council (NSERC) of Canada. The authors are sincerely thankful to NSERC, Canada.

References

1. Dilshad Masih, Yuanyu Ma, and Sohrab Rohani (2017) Graphitic C_3N_4 based noble-metal-free photocatalyst systems: A review. Applied Catalysis B: Environmental 206: 556-588.
2. Jiuqing Wen, Jun Xie, Xiaobo Chen, and Xin Li (2017) A review on g-C_3N_4-based photocatalysts. Applied Surface Science 391: 72-123.
3. Ong Wee-Jun, Lling-Lling Tan, Yun Hau Ng, Siek-Ting Yong, Siang-Piao Chai (2016) Graphitic Carbon Nitride (g-C_3N_4)-Based Photocatalysts for Artificial Photosynthesis and Environmental Remediation: Are We a Step Closer To Achieving Sustainability? Chemical Reviews 116: 7159-7329.
4. Fujishima Akira, and Kenichi Honda (1972) Electrochemical Photolysis of Water at a Semiconductor Electrode. Nature 238: 37-38.
5. Xinchen Wang, Kazuhiko Maeda, Arne Thomas, Kazuhiro Takanabe, Gang Xin, et al. (2009) A metal-free polymeric photocatalyst for hydrogen production from water under visible light. Nature Materials 8: 76-80.
6. Savio JA Moniz, Stephen A Shevlin, David James Martin, Zheng-Xiao Guo, Junwang Tang (2015) Visible-light driven heterojunction photocatalysts for water splitting – a critical review. Energy & Environmental Science 8: 731-759.
7. Ian Sullivan, Brandon Zoellner, Paul A Maggard (2016). Copper(I)-Based p-Type Oxides for Photoelectrochemical and Photovoltaic Solar Energy Conversion. Chemistry of Materials 28: 5999-6016.
8. Adriana Paracchino, Vincent Laporte, Kevin Sivula, Michael Grätzel, Elijah Thimsen. 2011. Highly active oxide photocathode for photoelectrochemical water reduction. Nature Materials 10: 456-461.
9. Moussab Harb, Dilshad Masih, Samy Ould-Chikh, Philippe Sautet, Jean-Marie Basset, et al. (2013) Determination of the Electronic Structure and UV–Vis Absorption Properties of (Na_2–xCux)Ta_4O_{11} from First-Principle Calculations. The Journal of Physical Chemistry C 117: 17477-17484.
10. Moussab Harb, Dilshad Masih, Kazuhiro Takanabe (2014) Screened coulomb hybrid DFT investigation of band gap and optical absorption predictions of $CuVO_3$, $CuNbO_3$ and $Cu_5Ta_{11}O_{30}$ materials. Physical Chemistry Chemical Physics 16: 18198-18204.
11. Sambandam Anandan, Jerry J Wu, Detlef Bahnemann, Alexei Emeline, Muthupandian Ashokkumar (2017) Crumpled Cu_2O-g-C_3N_4 nanosheets for hydrogen evolution catalysis. Colloids and Surfaces A: Physicochemical and Engineering Aspects 527: 34-41.
12. Anuradha Mitra, Promita Howli, Dipayan Sen, Biswajit Das, Kalyan Kumar Chattopadhyay (2016) Cu_2O/g-C_3N_4 nanocomposites: an insight into the band structure tuning and catalytic efficiencies. Nanoscale 8: 19099-19109.
13. Yanlong Tian, Binbin Chang, Jie Fu, Baocheng Zhou, Jiyang Liu, et al. (2014) Graphitic carbon nitride/Cu_2O heterojunctions: Preparation, characterization, and enhanced photocatalytic activity under visible light. Journal of Solid State Chemistry 212: 1-6.
14. Jie Chen, Shaohua Shen, Penghui Guo, Meng Wang, Po Wu, et al. (2014) In-situ reduction synthesis of nano-sized Cu_2O particles modifying g-C_3N_4 for enhanced photocatalytic hydrogen production. Applied Catalysis B: Environmental 152: 335-341.
15. Li Liu, Yuehong Qi, Jinshan Hu, Weijia An, Shuanglong Lin, et al. (2015) Stable Cu_2O@g-C_3N_4 core@shell nanostructures: Efficient visible-light photocatalytic hydrogen evolution. Materials Letters 158: 278-281.
16. Lixia Wang, Fei Zhao, Qing Han, Chuangang Hu, Lingxiao Lv, et al. (2015) Spontaneous formation of Cu_2O–g-C_3N_4 core–shell nanowires for photocurrent and humidity responses. Nanoscale

7: 9694-9702.
17. Ziyan Min, Xipeng Wang, Yaping Li, Jianbo Jiang, Jun Li, et al. (2017) A highly efficient visible-light-responding Cu_2O–TiO_2/g-C_3N_4 photocatalyst for instantaneous discolorations of organic dyes. Materials Letters 193: 18-21.
18. Yongchao Bao, Kezheng Chen (2017) A novel Z-scheme visible light driven Cu_2O/Cu/g-C_3N_4 photocatalyst using metallic copper as a charge transfer mediator. Molecular Catalysis 432: 187-195.
19. Anup Kumar Sasmal, Soumen Dutta, Tarasankar Pal (2016) A ternary Cu_2O–Cu–CuO nanocomposite: a catalyst with intriguing activity. Dalton Transactions 45: 3139-3150.
20. Piyong Zhang, Tingting Wang, Heping Zeng (2017) Design of Cu-Cu_2O/g-C_3N_4 nanocomponent photocatalysts for hydrogen evolution under visible light irradiation using water-soluble Erythrosin B dye sensitization. Applied Surface Science 391: 404-414.
21. Mamiko Kamiya, Mika Eguchi, Takashi Miura, Tomiya Kishi (1998) Lithium insertion behaviour of α-$CuVO_3$. Solid State Ionics 109: 321-326.
22. Barrier N, Hervieu M, Nguyen N, Raveau B (2008) Example of unusual tetrahedral coordination of Cu(I) in oxides: Cu_3VO_4. Solid State Sciences 10: 137-140.
23. Trimarchi, Giancarlo, Haowei Peng, Jino Im, Arthur J Freeman, Veerle Cloet, Adam Raw, Kenneth R. Poeppelmeier, Koushik Biswas, Stephan Lany, and Alex Zunger. 2011. Using design principles to systematically plan the synthesis of hole-conducting transparent oxides: Cu_{3} VO_{4} and Ag_{3} VO_{4} as a case study. Physical Review B 84: 165116.
24. Prangya P Sahoo, Brandon Zoellner, Paul A Maggard (2015) Optical, electronic, and photoelectrochemical properties of the p-type Cu_3−x VO_4 semiconductor. Journal of Materials Chemistry A 3: 4501-4509.
25. Qinqin Liu, Chunya Fan, Hua Tang, Xiujuan Sun, Juan Yang, et al. (2015) One-pot synthesis of g-C_3N_4/V_2O_5 composites for visible light-driven photocatalytic activity. Applied Surface Science 358. 188-195.
26. Yan SC, Li ZS, Zou ZG (2009) Photodegradation Performance of g-C_3N_4 Fabricated by Directly Heating Melamine. Langmuir 25: 10397-10401.
27. Shuying Dong, Jinglan Feng, Maohong Fan, Yunqing Pi, Limin Hu, et al. (2015) Recent developments in heterogeneous photocatalytic water treatment using visible light-responsive photocatalysts: a review. RSC Advances 5: 14610-14630.
28. Sulagna Patnaik, Satyabadi Martha, Parida KM (2016) An overview of the structural, textural and morphological modulations of g-C_3N_4 towards photocatalytic hydrogen production. RSC Advances 6: 46929-46951.
29. Yukun Shi, Xiaojing Hu, Jingtao Zhao, Xiaojiao Zhou, Baolin Zhu, et al. (2015) CO oxidation over Cu_2O deposited on 2D continuous lamellar g-C_3N_4. New Journal of Chemistry 39: 6642-6648.
30. Ganesh Babu S, Vinoth R, Surya Narayana P, Detlef Bahnemann, Neppolian B (2015) Reduced graphene oxide wrapped Cu_2O supported on C_3N_4: An efficient visible light responsive semiconductor photocatalyst. APL Materials 3: 104415.